RSC Advances

This article can be cited before page numbers have been issued, to do this please use: I. Leu, M. Hon and J. Tsai, *RSC Adv.*, 2014, DOI: 10.1039/C4RA10584B.

ROYAL SOCIETY OF CHEMISTRY

www.rsc.org/advances

View Article Online
DOI: 10.1039/C4RA10584B

Graphical abstract

Colour graphic:

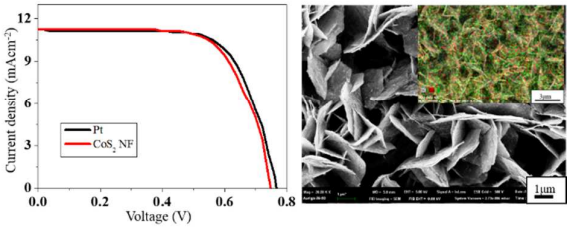

Text:

CoS_2 nanoflake arrays were fabricated on TCO for the counter electrode in DSSC application.

View Article Online
DOI: 10.1039/C4RA10584B

Journal Name

RSCPublishing

ARTICLE

Preparation of CoS_2 nanoflake arrays through ion exchange reaction of $Co(OH)_2$ and their application as counter electrode for dye-sensitized solar cell

Jung-che Tsai,[a] Min-hsiung Hon [a,b] and Ing-chi Leu [c,*]

Cite this: DOI: 10.1039/xoxxoooooox

Received ooth January 2012,
Accepted ooth January 2012

DOI: 10.1039/xoxxoooooox

www.rsc.org/

The cobalt sulfide nanoflake arrays prepared by the transformation of $Co(OH)_2$ nanoflake arrays using the ion exchange reaction method were incorporated into Pt-free dye-sensitized solar cells (DSSCs). Morphologies and crystal structures of the cobalt sulfide and cobalt hydroxide nanoflakes arrays were characterized by SEM, TEM and XRD analyses, respectively. The electrochemical properties were determined by cyclic voltammetry (CV) measurement. The cobalt sulfide nanoflakes which composed of CoS_2 single crystals and their aggregates dispersing in the amorphous cobalt sulfide matrix were completely transferred by substitution of S^{2-} for O^{2-} in the ion exchange reaction. The DSSC assembled with cobalt sulfide nanoflake arrays as the counter electrode showed a photovoltaic conversion efficiency of 5.20%, which was close to that of DSSC with sputtered Pt as the counter electrode (5.34%). Therefore, the cobalt sulfide nanoflake array film can be considered as a promising alternative counter electrode for use in DSSCs due to its large surface area and high electrocatalytic performance.

Introduction

Dye-sensitized solar cells (DSSCs) have received a lot of attention due to their low cost, relatively high performance and easy fabrication process[1]. Generally, a typical DSSC consists primarily of a photoanode, an electrolyte and a counter electrode. A conventional photoanode used is a dye-sensitized porous titania (TiO_2) on FTO (SnO_2:F) coated glass. During the photovoltaic process, photoelectrons generated from the excited state dyes are injected into the conduction band of TiO_2 and further transferred across external circuit to counter electrode. Meanwhile, the remained holes in oxidized dyes are regenerated by I^- in the electrolyte. Then the resultant I_3^- ions diffuse to the surface of counter electrode and reduce to I^- by receiving the external circuit electron for completing the continuous loops of dye regeneration and photoelectron injection. The most common material for counter electrodes is platinum (Pt) deposited on FTO coated glass due to its superior electrocatalytic activity for the I_3^-/I^- redox couple, the electrical conductivity and reliability[2]. However, the high price noble metal Pt as the counter electrode restricts DSSCs large-scale manufacture and their widespread application. So far, many reports have been carried out to search for cheaper and effective substitutes for Pt in counter electrodes.

Carbonaceous materials (carbon black[3], graphene[4], carbon nanotubes[5], etc.) and conductive polymers (PEDOT[6], polypyrrole[7], etc.) were investigated as counter electrode materials of DSSCs for their good catalytic capability and conductivity. Some catalytically active transition metal compounds such as carbides[8], nitrides[9], oxides[10] and various hybrids[3] have been shown to have a great potential to replace Pt due to the intrinsic catalytic activity for I_3^- reduction and the various morphologies to offer high specific surface. Compared to carbonaceous or polymer materials, inorganic materials have unique properties such as low cost, material diversity, abundance, high catalytic activity and ease of modification. Recent reports showed that some catalytic metal sulfides such as MoS_2[11], WS_2[11], NiS[12], and CoS[13] also can serve as efficient catalytic counter electrodes of DSSCs owing to their outstanding catalytic capability and abundant feedstock. In 2009, CoS electrodeposited on the flexible substrate showed comparable catalytic activity to Pt as the counter electrodes, which opened up the way to exploring more transition meal sulfides[13]. It is well known that a high specific surface area is beneficial for providing more active sites of counter electrodes. The hierarchical CoS spindles in the counter electrodes in DSSCs have been reported to have a high catalytic activity[14]. However, it is known that the electrochemical properties are determined by the kinetic features controlled by the transport of electrons and ions into the active materials. It is an effective approach to enhance the kinetic features by directly constructing the nanoarray electrodes on the collector (FTO substrate). The deposited architecture provides an effective diffusion path for ions, and a lower internal resistance to realize the subsequent high-power performance. A large variety of approaches have been reported for synthesis of cobalt sulfides, such as electrochemical deposition[13], thermal decomposition method[15], hydrothermal method[16], and solvothermal method[17]. These methods are suitable for powder materials, but difficult to directly synthesize oriented cobalt sulfide nanostructures on the FTO. Therefore, it is of a great interest to develop a facile synthesis method for cobalt sulfide nanostructures for energy applications.

ARTICLE View Article Online DOI: 10.1039/C4RA10584B Journal Name

The solution-based ion exchange reaction (IER) has been proven to be a low-cost and effective method for chemical transformation of nanomaterials into dedicated composition and morphology[18]. The solution-based IER avoids the disadvantages of high temperatures, high pressure and toxic gas sources such as H_2S. At the same time, it reduces the danger and cost of the fabrication process. Conventionally, the different nanostructures of metal sulfides such as nickel sulfide or cobalt sulfide have been derived from nanostructures of metal oxides or hydroxides[19]. During the IER process, cobalt sulfide nanostructures were transformed from Co_3O_4 nanostructures and maintained the morphologies of metal oxides[19]. Therefore, IER is a promising technique to synthesize the metal sulfides for energy applications. To date, there are only a limited number of reports on nanoflakes of cobalt sulfide grown directly on FTO substrate because their cobalt hydroxide precursor is usually synthesized in solution or on the nickel foam. In the present work, cobalt hydroxide is used as the skeleton to be transformed into cobalt sulfide via the IER method. As a result of shape-preserved reaction, the CoS_2 nanoflake arrays were fabricated from $Co(OH)_2$ nanoflake arrays and retained strong contact with the FTO substrate. It is found that the CoS_2 nanoflake arrays exhibit outstanding I^-/I_3^- redox catalytic activity and a power conversion efficiency of 5.2% is achieved for the DSSC with CoS_2 nanoflake arrays as the counter electrode, which is nearly as that of the DSSC with sputtered Pt as the counter electrode (5.34%).

Experimental

Chemicals

Cobalt acetate 9-hydrate ($Co(CH_3COO)_2{\cdot}9H_2O$, 98%), cobalt sulfate ($CoSO_4{\cdot}9H_2O$, 99%), sodium sulfide 9-hydrate ($Na_2S{\cdot}9H_2O$, 98%), and hexamethylenetetramine ($C_6H_{12}N_4$, HMTA, 99%) were obtained from Sigma-Aldrich. Titania nanoparticles (P25, size: ~21nm, 20% rutile and 80% anatase) and Di-tetrabutylammonium cis-bis(isothiocyanato)bis(2,2'-bipyridyl-4,4'-dicarboxylato)ruthenium(II) (N719, $C_{58}H_{86}N_8O_8RuS_2$, 99.9%) were purchased from UniRegion Bio-Tech. Inc.. Anhydrous lithium iodide (LiI, >98%), lithium perchlorate, ($LiClO_4$, >99.8%), iodine (I_2, >98%), tert-butanol ($C_4H_{10}O$, 99.9%) and acetonitrile (CH_3CN, ACN, 99.9%) were obtained from Alfa Aesar. 1.3-dimethylimidazolium iodine ($C_5H_9IN_2$, 99.8%), 4-tert-butylpyridine ($C_9H_{13}N$, 99.8%), guanidine thiocyanate (CH_6ClN_3, 99.8%) were purchased from Merck. Ethanol (99.5%) was purchased from J. T. Baker. De-ionized water was used throughout the work.

Preparation of CoS_2 nanoflake array films

The experimental details are as follows. Clean FTO glasses with 1 cm × 2 cm in size were used as substrates. To facilitate the nucleation of $Co(OH)_2$ nanoflake arrays, a 5 nm-thick Co_3O_4 thin film (seed layer) was first deposited on the FTO substrate by spin coating a 5 mM ethanolic solution of cobalt acetate, followed by conversing to Co_3O_4 at 350℃ for 30 min in air[20]. In a hydrothermal synthesis of $Co(OH)_2$ nanoflake array film, 0.1 M cobalt acetate and 0.3 M hexamethylenetetramine were dissolved in 20 mL of deionized water to form a homogeneous solution with pink color, which was transferred into the teflon-lined stainless steel autoclave. After that, the pieces of FTO glass substrate were immersed into the reaction solution with an angle against the wall. Then, the autoclave was sealed and maintained at 120℃ for 0.5~5 h in an electric oven. After cooling down to room temperature naturally, the samples were fetched out and washed with deionized water. To transform the hydroxide into cobalt sulfide, the ion exchange reaction was performed on the samples by rinsing in 0.1 M sodium sulfide aqueous solution at 75℃ for 8 h.

Fabrication of the DSSCs

The TiO_2 paste prepared by mixing P25, ethanol, DI-water and X100 was coated on a cleaned FTO substrate by the doctor-blade method. The TiO_2 electrode (~20μm) was gradually heated to 450℃ (rate = 5℃/min) and subsequently sintered at that temperature for 30 min. After cooling it to 80℃, the electrode was dipped in a solution containing 0.3 mM N719 dye in a mixed solvent of acetonitrile and tert-butanol in a volume ratio of 1:1 for a day. The dye-sensitized TiO_2 electrode was coupled with the various cobalt sulfide electrodes (or sputtered Pt electrode for comparison) to fabricate the DSSCs. These two electrodes were separated by a 60 μm thick thermal plastic Surlyn film and sealed by heating. A mixture of 1 M 1.3-dimethylimidazoliumiodine (Merck), 0.5 M 4-tert-butylpyridine, 0.15 M iodine, and 0.1 M guanidine thiocyanate in ACN was used as the electrolyte and injected into the gap between the two electrodes by capillarity. An area of 0.237 cm^2, defined by a metal mask, was selected as the active region for the photovoltaic measurement. The symmetrical cell was composed of two identical electrodes and its electrochemistry measurement had the same conditions and arrangement as the DSSCs.

Characterization

The surface morphology and composition of cobalt hydroxide and cobalt sulfide were characterized by field-emission scanning electron microscopy (FESEM, Auriga 39-50, Zeiss) equipped with an energy dispersive X-ray spectrometer (EDX, XFlash 5030, Bruker). X-ray diffraction experiments were carried out with an automatic X-ray powder diffractometer (D/MAX2500, Rigaku). The transmission electron microscopy (TEM) images were obtained from a high-resolution analysis electron microscope (HRAEM, JEM-2100F CS STEM, JEOL) with an accelerating voltage of 200 kV. Cyclic voltammetry (CV) measurement was carried out in a three-electrode system in an acetonitrile solution contained 0.1 M $LiClO_4$, 10 mM LiI and 1 mM I_2 at a scanning rate of 50 mV/s using an electrochemical analyzer (263A, EG&G). Pt worked as the counter electrode and Ag/Ag^+ worked as the reference electrode. Tafel-polarization curves of the symmetrical cells were measured by the same electrochemical analyzer. The photovoltaic performance of the DSSCs was studied under simulated AM 1.5 illumination (100 mW/cm^2, Sol2A Class ABA Solar Simulators, Oriel) with a digital source meter (Model 2400, Keithley). In addition, the incident light illuminated from the photoanode (working electrode) side and its intensity was calibrated with a standard Si-based solar cell (9115DV, Oriel).

Results and discussion

The cobalt sulfide nanoflake arrays are transformed from the $Co(OH)_2$ nanoflake arrays first prepared on the FTO glass, therefore

Journal Name
View Article Online
DOI: 10.1039/C4RA10584B
ARTICLE

it is important to know the growth characteristics of the $Co(OH)_2$ nanoflake arrays. To investigate the growth of $Co(OH)_2$ nanoflake arrays, the hydrothermal synthesis method was kept at 120 ℃ for different growth time. The reactions involved in the hydrothermal synthesis of $Co(OH)_2$ nanoflake arrays can be illustrated as follows[21].

$$C_6H_{12}N_4 + 6H_2O \rightarrow 6HCHO + 4NH_3 \quad (1)$$

$$NH_3 + H_2O \leftrightarrow NH_4^+ + OH^- \quad (2)$$

$$Co^{2+} + 2OH^- \rightarrow Co(OH)_2 \quad (3)$$

At the growth time of 0.5 h, the random nucleated cobalt hydroxide reveals dark spots on the FTO surface, which is shown in figure 1 (b) SEM image. When HMTA is continuously thermally decomposed to generate more OH^-, the tiny flake structures are grown from the nucleate sites. After prolonging the growth time, neighboring flakes become larger and are bound together by weak Van der Waal force to form the nanoflake arrays. Finally, the surface of FTO was covered by the $Co(OH)_2$ nanoflake arrays. The as-deposited film is uniform in appearance and exhibits bluish-green in color. It is reported in the literature that cobalt hydroxides prefer to grow into nanoflakes which align vertically to the substrate due to their intrinsic lamellar structure[22]. Because $Co(OH)_2$ has a layered brucite crystal structure of the CdI_2 type, which shows a weak interaction between layers and strong binding within the layered planes[16]. The two-dimensional monolayer consists of edge-shared CoO_6 octahedrons [23]. Therefore, (001) plane of $Co(OH)_2$ is stable with the lowest surface energy and $Co(OH)_2$ will preferentially grow along the layered plane to form two-dimensional nanoflake array films[24].

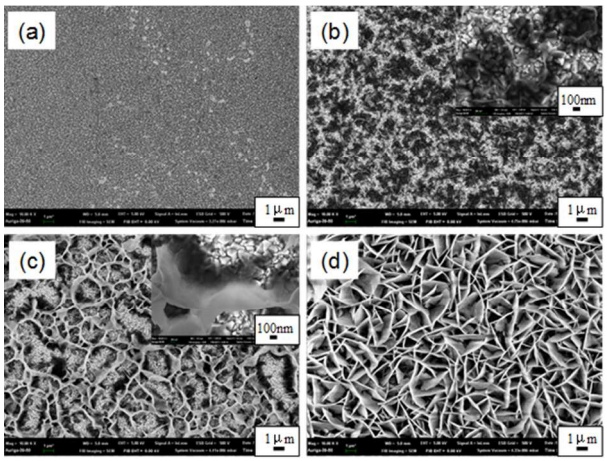

Fig. 1 SEM images of $Co(OH)_2$ nanoflake arrays on FTO substrate via a hydrothermal synthesis at 120 ℃ for (a)0, (b)0.5, (c)1, and (d) 5 h.

The SEM top-view and cross-section images of the hydrothermally synthesized $Co(OH)_2$ nanoflake arrays for 5 h are shown in figure 2 (a) and (b). The $Co(OH)_2$ films exhibit a highly porous structure with pore diameter ranging from 20 nm~1 μm and its height is about 4.4 μm. The synthesized $Co(OH)_2$ film has a network of interconnected nanoflake arrays with a thickness of 20 nm. It is believed that this porous feature is helpful to enhance the follow-up IER process and the resulting performance of devices. During the cross-section preparation of samples, the nanoflake arrays did not detach from the substrate and basically maintained the original structure at the action of the strong shearing stress. Impressively, it is also indicated that $Co(OH)_2$ nanoflake array film has a good adhesion with the FTO substrate in the high magnification SEM image, which is shown as inset of figure 2 (b). Figures 2 (c) and (d) are TEM analyses of scraped $Co(OH)_2$ nanoflake from FTO substrate. TEM image shows that the individual nanoflake has a smooth feature. Additionally, 6-fold symmetric diffraction spots in the nano beam electron diffraction pattern (NBDP) (inset of figure 2 (c)) for the nanoflake can be indexed with the α-$Co(OH)_2$ phase, and a high resolution

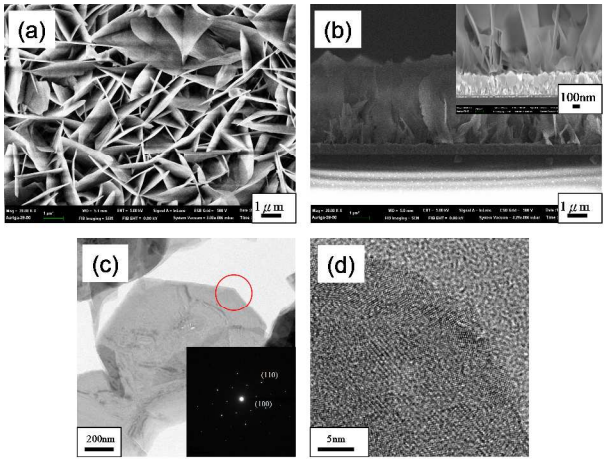

TEM image shows that the α-$Co(OH)_2$ nanoflake is polycrystalline in nature.

Fig. 2 (a) and (b) SEM images of $Co(OH)_2$ nanoflake arrays on FTO substrate. (c) TEM image and (d) High resolution TEM image of a scraped $Co(OH)_2$ nanoflake (NBDP in sect).

The XRD pattern indicates that highly crystalline α-$Co(OH)_2$ is formed without other crystal phases, as shown in figure 3 (b). It reveals a predominant brucite-like phase in which the 2θ scan has peaks at 12.4°, 21.3°, 32.9°, 35.3°, and 58.8°, corresponding to the (003), (006), (101), (012), and (110). The other peaks belong to the peaks of FTO substrate, which match the diffraction peaks in figure 3 (a). The result of XRD conforms the results obtained in a previous study[25]. The cobalt hydroxide has two phases that α-phase is in bluish-green color and β-phase is in red-pink color. The XRD results also match the as-prepared $Co(OH)_2$ nanoflake arrays with bluish-green color in the present work. After IER process, the peaks of α-$Co(OH)_2$ XRD pattern disappear but those of FTO pattern remain in figure 3 (c). It is a clear evidence of transformation from $Co(OH)_2$ nanoflake arrays to cobalt sulfide nanoflake arrays. The details of

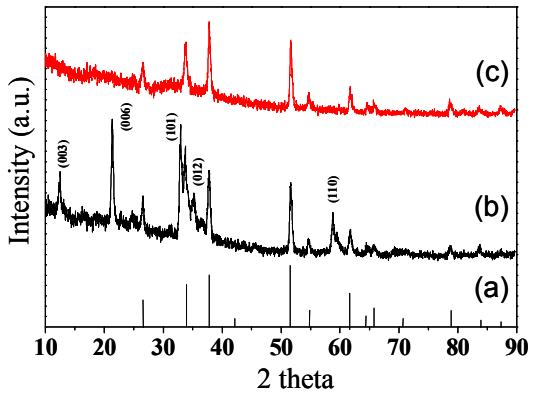

View Article Online
DOI: 10.1039/C4RA10384B
Journal Name

cobalt sulfide phase will be discussed in figure 4.

Fig. 3 XRD patterns of (a) FTO substrate, (b) as-prepared $Co(OH)_2$ nanoflake array film and (c) $Co(OH)_2$ nanoflake array film after the IER method at 75 ℃ for 8 h.

The SEM image of the cobalt sulfide nanoflake array films is shown in figure 4 (a). Compared to the $Co(OH)_2$ nanoflake arrays with a relatively smooth surface (figure 2 (a)), it can be seen that the cobalt sulfide nanoflake arrays remain the same nanoflake morphology but surface of nanoflakes becomes rougher after the IER process. This observation provides the evidence that the IER method does not damage the basic morphology of the nanoflake arrays. During the IER method, the substitution of S^{2-} for O^{2-} occurs when the S^{2-} source contacts with the $Co(OH)_2$ surface. It can be thought that the IER method is a diffusion controlled process, so the nanoflake structure will be rarely damaged. Therefore, nanoflake array structure is suitable for IER method because of short distance diffusion from surface to center in a piece of nanoflake. Using the EDS mapping technique, it reveals that Co (red dots) and S (green dots) are homogeneously spread over the whole nanoflake structure. Figures 4 (c)-(e) show the TEM analyses of the nanoflakes scrapped from the film of cobalt sulfide nanoflake arrays. The TEM result indicates that the tranformed cobalt sulfide nanoflakes exhibit CoS_2 single crystals and aggregates dispersing in the amorphous cobalt sulfide matrix. From element ratio of EDS and NBDP analyses, the tiny grains are CoS_2 phase. Interestingly, the high resolution TEM image (figure 4 (e)) shows that cobalt sulfide nanoflakes are composed of CoS_2 crystals and amorphous cobalt sulfide. The EDS analyses of specific areas on the single CoS_2 nanoflake are shown in figure S1.This result shows that there are no obvious peaks of cobalt sulfide in the XRD pattern because the intensity of CoS_2 peaks is too weak to be detected or hidden under the background noise, i.e., the amount of CoS_2 is below the detection limit of XRD, while the major component in the matrix is the amorphous sulfide phase.

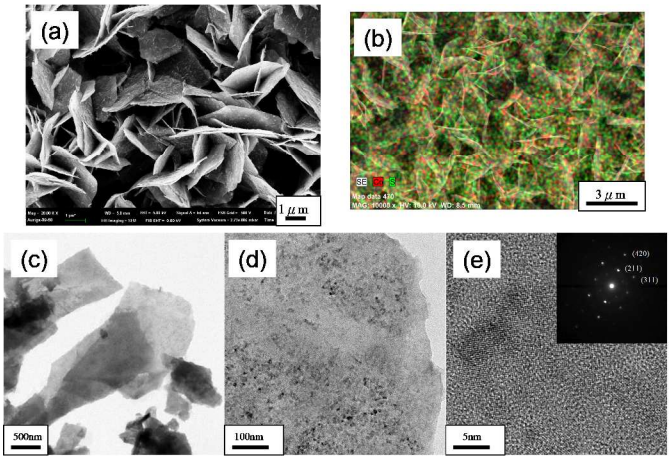

Fig. 4 (a) The SEM image and (b) EDS element mapping of CoS_2 nanoflake arrays on FTO substrate. (c)-(e) TEM analyses of scrapped CoS_2 nanoflakes (NBDP in inset).

The synthesis mechanism of cobalt sulfides using the IER method is proposed based on the difference of the solubility product constant (K_{sp}) of the materials. A material with lower K_{sp} value is more thermodynamically stable than that with higher K_{sp} value[18]. For example, the K_{sp} values of $Co(OH)_2$, Co_3O_4 and CoS are about 5.9×10^{-15}, 3.1×10^{-18} and 3×10^{-26} , respectively[26]. It is believed that K_{sp} values of cobalt sulfides are much smaller than those of cobalt hydroxides and cobalt oxides. It is to say that the latter is tendentious to convert into the former by providing the excess sulfur source (like S^{2-}). In our studies, when the $Co(OH)_2$ samples are soaked into the Na_2S solution, the samples change the color from bluish-green to dark gray rapidly, which means that the ion exchange reaction occurs immediately. Therefore, the CoS_2 nanoflake arrays can be obtained by the ion exchange reactions from $Co(OH)_2$ nanoflake arrays in a solution containing S^{2-} anions. Additionally, previous studies have been reported that both thermodynamics and kinetics of IER method depended on the interface reaction between metal oxide (or hydroxide) and S^{2-} anions[27]. The reaction rate of nanostructured materials is much faster than that of bulky materials. Consequently, the nanoflake structure is beneficial for the IER method to exchange the anions due to their high surface areas and short distance of diffusion.

To characterize the catalytic activity of the cobalt sulfide nanoflake arrays electrode toward the reduction of I_3^-, cyclic voltammetry (CV) experiments were carried out. For comparison, the CV of the sputtered Pt electrode was measured under the same conditions. Figure 5 shows the CVs of the CoS_2 nanoflake arrays and Pt electrodes. Two typical pairs of redox peaks are observed, implying a high catalytic activity for the reduction of I_3^-. The relative negative pair is assigned to the oxidation and reduction of I^-/I_3^-[Eq. (4)], whereas the relative positive pair was assigned to the oxidation and reduction of I_2/I_3^-[Eq.(5)] according to the literature[28].

$$I_3^- + 2e^- \leftrightarrow 3I^- \qquad (4)$$

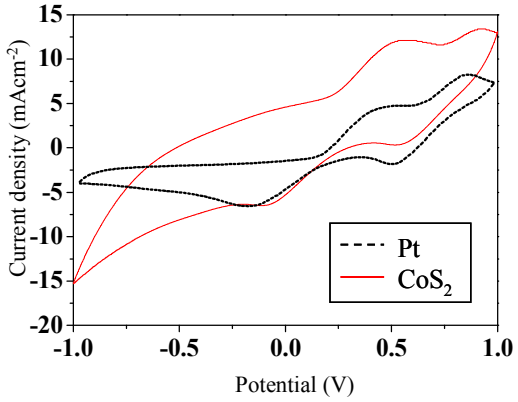

$$3I_2 + 2e^- \leftrightarrow 2I_3^- \qquad (5)$$

Fig. 5 Cyclic voltammograms of I_3^-/I^- for CoS_2 nanoflake arrays and sputtered Pt electrodes.

The profile and location of the two pairs of redox peaks for CoS_2 are almost similar to those of the Pt electrode, indicating that the former can behave a similar catalytic activity to the latter as a counter electrode in DSSCs. But the cathodic peak potential of the CoS_2 electrode is more positive than that of Pt electrode. It indicates that the overpotential for reduction of I_3^- to I^- of CoS_2 electrode is smaller than that of Pt electrode. And CoS_2 electrode exhibits larger current densities, which implies that surface area of CoS_2 electrode was larger than that of sputtered Pt electrode. For further investigation to verify the electrocatalytic capabilities of the counter electrodes, Tafel-polarization is measured using the symmetrical cells. Figure 6

View Article Online
DOI: 10.1039/C4RA10584B ARTICLE

demonstrates the Tafel curves of the cells based on the CoS_2 and sputtered Pt electrodes with the logarithmic current density (log J) as a function of the voltage. The slope of a tangent to the CoS_2 curve is similar to that of Pt, indicating that the two electrodes have the similar electrocatalytic activity.

The current density-voltage (J-V) behavior of DSSCs under one Sun illumination (AM 1.5, 100mWcm^{-2}) using sputtered Pt or CoS_2 nanoflake arrays as the counter electrodes is shown in figure 7, and the photovoltaic parameter of device performance is summarized in Table 1. Both the DSSCs with CoS_2 nanoflake arrays and sputtered Pt used as the counter electrodes produce power conversion efficiencies of 5.20% and 5.34%, and yield a high fill factor of 0.688 and 0.694, respectively, indicating the high catalytic activity for triiodide reduction. The counter electrode with CoS_2 nanoflake arrays is compared with other counter electrodes with cobalt sulfide reported in the literature. Different kinds of cobalt sulfide have been prepared and used as the catalyst on the counter electrode of a DSSC in the literature. The CoS films were prepared by the potentiostaic method[13] and honeycomb-like CoS films were obtained by the potentiodynamic method[29]. The power conversion efficiencies of the DSSC with CoS as counter electrodes were 6.5% and 6.01%, respectively. For the comparison, efficiencies of the DSSCs with Pt counter electrode were 6.5% and 5.71%, respectively. And it was also shown that a conversion efficiency of 7.67% was achieved by using the CoS acicular nanorod arrays as the counter electrode of DSSCs, which was near the efficiency of a DSSC with Pt counter

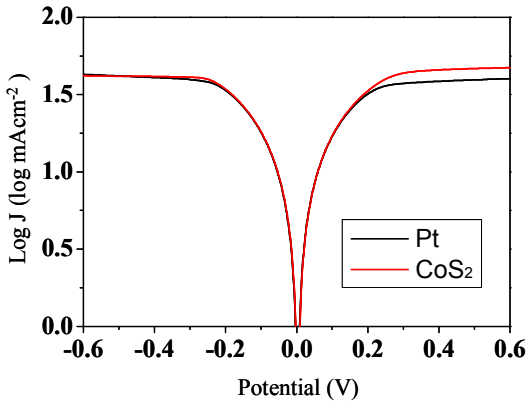

electrode (7.70%)[30]. It is noticed that the catalyst, electrolytes, and spacers in DSSCs are different in these cases and there is no perfectly comparable DSSC in the literature with DSSC in this study. The difference in efficiencies measured is within ~3% compared to the maximum efficiency obtained for each counter electrode in this study. The J-V performance of CoS_2 nanoflake arrays indicates that the cobalt sulfide nanostructure is an impressive counter electrode catalyst for I_3^-/I^- based DSSCs.

Fig. 6 Tafel polarization curves of the symmetrical cells based on CoS_2 nanoflake arrays and sputtered Pt electrodes.

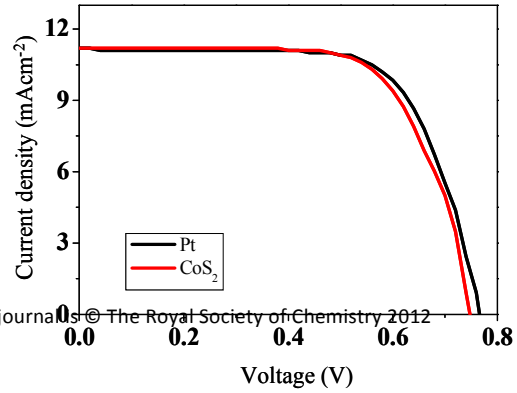

Fig. 7 Photocurrent density-voltage (J-V) curves of the DSSCs using sputtered Pt and CoS_2 nanoflake arrays as the counter electrodes.

Table 1 Photovoltaic parameters of the DSSCs using sputtered Pt and CoS_2 nanoflake arrays as the counter electrodes.

C.E.	V_{oc}(V)	J_{sc} (mAcm^{-2})	F.F.	η (%)
Sputtered Pt	0.767	10.04	0.694	5.34
CoS_2 nanoflake	0.747	10.13	0.688	5.20

Conclusions

In summary, the hydrothermal growth mechanism of $Co(OH)_2$ nanoflake arrays on FTO substrate is demonstrated in this work. Due to the difference of the solubility product constant, the polycrystalline CoS_2 nanoflake arrays were prepared via the solution-based ion exchange reaction without any damage to the basic morphology of the nanoflake arrays. The cobalt sulfide nanoflakes are composed of CoS_2 single crystals and their aggregates dispersing in the amorphous cobalt sulfide matrix. The introduction of nanoflake array structure as the counter electrodes leads to a large interfacial contact between the electrolyte and CoS_2 counter electrode, which is beneficial for the catalytic reaction of the I^-/I^{3-}. The synthesized film of CoS_2 nanoflake arrays was characterized using various electrochemical techniques and demonstrated the comparable catalytic activity as the counter electrode to sputtered Pt. The DSSC using CoS_2 nanoflake arrays as the counter electrode achieves a power conversion efficiency of 5.20%, which is close to the photovoltaic performance of DSSC using sputtered Pt as the counter electrode (5.34%). The low-cost, highly catalytic nanomaterial and facile fabrication method should have enormous potential to substitute the Pt counter electrode in the DSSCs.

Acknowledgements

We acknowledge the financial support of the Ministry of Science and Technology (MOST) grant funded by Taiwan government through MOST 103-2221-E-006-089 and NSC 102-2221-E-024-003 -MY3.

Notes and references

[a] Department of Materials Science and Engineering, National Cheng Kung University, Tainan, 701 Taiwan, R.O.C.
[b] Research Center for Energy Technology and Strategy, National Cheng Kung University, Tainan 701, Taiwan, R.O.C.
[c] Department of Materials Science, National University of Tainan, Tainan, 701 Taiwan, R.O.C. E-mail:icleu@mail.mse.ncku.edu.tw

1. B. Oregan and M. Gratzel, *Nature*, 1991, 353, 737-740.
2. A. Hauch and A. Georg, *Electrochim Acta*, 2001, 46, 3457-3466.

ARTICLE View Article Online DOI: 10.1039/C4RA10584B Journal Name

3. T. N. Murakami, S. Ito, Q. Wang, M. K. Nazeeruddin, T. Bessho, I. Cesar, P. Liska, R. Humphry-Baker, P. Comte, P. Pechy and M. Gratzel, *J Electrochem Soc*, 2006, 153, A2255-A2261.
4. J. D. Roy-Mayhew, D. J. Bozym, C. Punckt and I. A. Aksay, *Acs Nano*, 2010, 4, 6203-6211.
5. S. H. Seo, S. Y. Kim, B. K. Koo, S. I. Cha and D. Y. Lee, *Langmuir*, 2010, 26, 10341-10346.
6. J. B. Xia, N. Masaki, K. J. Jiang and S. Yanagida, *J Mater Chem*, 2007, 17, 2845-2850.
7. J. H. Wu, Q. H. Li, L. Q. Fan, Z. Lan, P. J. Li, J. M. Lin and S. C. Hao, *J Power Sources*, 2008, 181, 172-176.
8. M. X. Wu, X. A. Lin, A. Hagfeldt and T. L. Ma, *Angew Chem Int Edit*, 2011, 50, 3520-3524.
9. Q. W. Jiang, G. R. Li and X. P. Gao, *Chem Commun*, 2009, 7603-7603.
10. X. Lin, M. X. Wu, Y. D. Wang, A. Hagfeldt and T. L. Ma, *Chem Commun*, 2011, 47, 11489-11491.
11. M. X. Wu, Y. D. Wang, X. Lin, N. S. Yu, L. Wang, L. L. Wang, A. Hagfeldt and T. L. Ma, *Phys Chem Chem Phys*, 2011, 13, 19298-19301.
12. J. Yang, C. X. Bao, K. Zhu, T. Yu, F. M. Li, J. G. Liu, Z. S. Li and Z. G. Zou, *Chem Commun*, 2014, 50, 4824-4826.
13. M. K. Wang, A. M. Anghel, B. Marsan, N. L. C. Ha, N. Pootrakulchote, S. M. Zakeeruddin and M. Gratzel, *J Am Chem Soc*, 2009, 131, 15976-+.
14. G. Q. Wang and S. P. Zhuo, *Phys Chem Chem Phys*, 2013, 15, 13801-13804.
15. H. K. Mulmudi, S. K. Batabyal, M. Rao, R. R. Prabhakar, N. Mathews, Y. M. Lam and S. G. Mhaisalkar, *Phys Chem Chem Phys*, 2011, 13, 19307-19309.
16. W. J. Dong, X. B. Wang, B. J. Li, L. N. Wang, B. Y. Chen, C. R. Li, X. A. Li, T. R. Zhang and Z. Shi, *Dalton T*, 2011, 40, 243-248.
17. Q. R. Hu, S. L. Wang, Y. Zhang and W. H. Tang, *J Alloy Compd*, 2010, 491, 707-711.
18. L. Dloczik and R. Konenkamp, *Nano Lett*, 2003, 3, 651-653.
19. X. H. Xia, C. R. Zhu, J. S. Luo, Z. Y. Zeng, C. Guan, C. F. Ng, H. Zhang and H. J. Fan, *Small*, 2014, 10, 766-773.
20. X. H. Xia, J. P. Tu, Y. J. Mai, X. L. Wang, C. D. Gu and X. B. Zhao, *J Mater Chem*, 2011, 21, 9319-9325.
21. Z. Chen, Y. Chen, C. Zuo, S. Zhou, A. G. Xiao and A. X. Pan, *B Mater Sci*, 2013, 36, 239-244.
22. Y. L. Hou, H. Kondoh, M. Shimojo, T. Kogure and T. Ohta, *J Phys Chem B*, 2005, 109, 19094-19098.
23. Y. Oaki, S. Kajiyama, T. Nishimura and T. Kato, *J Mater Chem*, 2008, 18, 4140-4142.
24. X. H. Xia, J. P. Tu, J. Y. Xiang, X. H. Huang, X. L. Wang and X. B. Zhao, *J Power Sources*, 2010, 195, 2014-2022.
25. R. Z. Ma, Z. P. Liu, K. Takada, K. Fukuda, Y. Ebina, Y. Bando and T. Sasaki, *Inorg Chem*, 2006, 45, 3964-3969.
26. A. P. Miller, *Am J Public Health N*, 1941, 31, 1324-1324.
27. D. H. Son, S. M. Hughes, Y. D. Yin and A. P. Alivisatos, *Science*, 2004, 306, 1009-1012.
28. C. H. Yoon, R. Vittal, J. Lee, W. S. Chae and K. J. Kim, *Electrochim Acta*, 2008, 53, 2890-2896.
29. J. Y. Lin, J. H. Liao and T. C. Wei, *Electrochem Solid St*, 2011, 14, D41-D44.
30. C. W. Kung, H. W. Chen, C. Y. Lin, K. C. Huang, R. Vittal and K. C. Ho, *Acs Nano*, 2012, 6, 7016-7025.

